Fractal growth of a conventional calamitic liquid crystal

I. Dierking,* H. K. Chan, F. Culfaz, and S. McQuire
Schuster Laboratory, Department of Physics and Astronomy, University of Manchester, Oxford Road, Manchester M13 9PL, United Kingdom
(Received 21 April 2004; published 4 November 2004)

We report observation of liquid crystal phase ordering via fractal growth aggregates for a calamitic, nonbent-core mesogen. Fractal growth of a conventional smectic-*C* (Sm-*C*) phase from the isotropic melt after a temperature quench was experimentally investigated with respect to time, cell gap, quench depth, and quench rate. The determined fractal dimensions relating to the area as well as the perimeter of the growing aggregates suggest a phase formation process via a percolation mechanism. Computer simulations of the phase ordering process give further evidence for percolation growth, qualitatively reproducing the observed textures and quantitatively leading to the same fractal dimensions. We propose a general model of fractal smectic liquid crystal growth, which accounts for all of the different systems observed so far, bent-core or "banana" phases as well as the observation of fractal phase ordering of a conventional Sm-*C* phase. The model is based on the "breaking" of the commonly observed growth anisotropy by strong in-layer molecular interactions. These are provided by hydrogen bonding in the Sm-*C* case discussed here and by steric interactions in the case of the bent-core phases discussed in previous publications.

DOI: 10.1103/PhysRevE.70.051701 PACS number(s): 61.30.−v, 61.43.Hv, 64.60.Ak, 64.70.Md

I. INTRODUCTION

Nucleation, growth, aggregation, coalescence, and domain coarsening have been topics of long-standing scientific interest in condensed-matter, solid-state, and soft-matter physics [1]. This is related not only to the question of developing a unified theoretical understanding [2,3] of the formation and phase ordering kinetics of a large variety of different systems, but is also of most eminent practical importance—for example, from alloy production all the way to pharmaceutical synthesis. Essentially, the mechanical, electric, magnetic, and optical properties of many materials classes depend on the way they are produced—i.e., in general, on thermal history and the respective phase ordering dynamics. In comparison to the large number of investigations that have been carried out on liquid and solid systems over the last century, phase ordering studies on liquid crystals are relatively rare, despite the fact that phase formation can often quite easily be followed experimentally by use of a polarization microscope and adequate image acquisition.

Growth in condensed-matter systems can take a variety of different forms [4,5], ranging from the production of large, near-to-perfect single crystals in the semiconductor industry, spherulitic growth in the crystallization of polymers, and the formation of dendrites all the way to fractal structures, predominantly observed in soft-matter materials such as colloids and polymers [6,7]. Only very recently has fractal growth in liquid crystals been reported [8], which was observed in the phase ordering processes of various novel phases related to bent-core mesogens, the so-called "banana" phases [9–11]. Fractal aggregates of banana phases have been reported for isothermal growth at the transition from the isotropic to the *B*2 [12] as well as the *B*7 [13] phase, both phases being somewhat similar to the fluid smectic phases of conventional calamitic mesogens, while the latter generally grow via nonfractal smectic bâtonnets to form fan-shaped textures [14]. Growth via fractal aggregates has also been reported for the crystallization of bent-core molecules—i.e., the transition into the *B*4 phase [15,16]. In all these cases of liquid crystal banana phase ordering, complex growth structures were observed, which are qualitatively different from those exhibited by conventional calamitic phases. So are those observed in the present investigation, reporting observation of the fractal growth of a nonbanana mesogen. The aim of this paper is to provide a general description of fractal growth structures in liquid crystals by a simple generic growth model. This offers general new insights into the microscopic phase ordering mechanism of mesogens forming fractal aggregates.

Analysis of complex patterns by fractal geometric methods [17] has been proven a valuable tool in the description of complicated structures in many areas of science, ranging from physics, chemistry, and biology all the way to material science and geology [18–20]. Valuable information about the underlying growth mechanism can be extracted from the fractal dimension of such structures and aggregates, relating to three fundamental growth models: diffusion-limited aggregation (DLA) [21], cluster-cluster aggregation (CCA) [22], and percolation [23,24]. The model of diffusion-limited aggregation is based on single particles performing random walks before joining a single growing aggregate. The expected fractal dimension of such an aggregate is about $D=1.7$ in two-dimensional space, which, for example, describes well the process of electrodeposition. Cluster-cluster aggregation involves the random motion of many particles at the same time, sticking together to form clusters which continue to perform random walks until eventually all particles are part of one single aggregate. The fractal dimension of CCA clusters generally varies between $D=1.6$ and 1.8 in two-dimensional space, depending strongly on experimental

*Corresponding author.
Electronic address: dierking@reynolds.ph.man.ac.uk

or simulation conditions, such as the sticking probability. Processes described are, for example, found in the aggregation of colloids or wax spheres floating on water. Both of these models, DLA and CCA, do not apply to the current experimental situation, as we do not have individual particles (ions, colloids) performing random walks, but rather observe a nucleation and growth process, where individual nuclei do not move. In all cases of fractal liquid crystal growth, banana phase ordering as well as the results reported in the present study of a hydrogen-bonded calamitic mesogen, a saturation fractal dimension of $D=1.9$, has been observed so far. This is clearly different from those of the above-outlined growth mechanisms and indicates growth via site percolation at the percolation threshold for which a fractal dimension of $D=91/48=1.896$ is expected theoretically.

Here we report an analysis of fractal growth aggregates from a conventional calamitic mesogen. We demonstrate that the observed structures exhibit the same fractal dimension of $D=1.9$ as those shown by the previously investigated banana mesogens. Based on a simple model of broken growth anisotropy due to large lateral intermolecular interactions, we demonstrate that all experimentally observed fractal growth aggregates and textures of liquid crystals can be simulated by percolation growth at the percolation threshold.

II. EXPERIMENT

A. General experimental conditions

The compound investigated in this study is bis-(4-*n*-octyloxybenzoyl)hydrazine [25–27], abbreviated as 8DBH. Its structural formula is

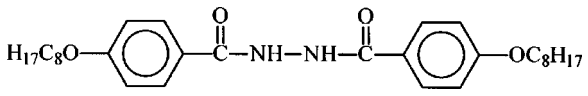

The phase sequence of 8DBH on cooling, as determined by polarizing microscopy, is

$$\text{iso} \overset{\leftrightarrow}{177\,^\circ\text{C}} \text{Sm-}C \overset{\leftrightarrow}{175\,^\circ\text{C}} \text{cub} \overset{\leftrightarrow}{131\,^\circ\text{C}} \text{cryst} \qquad (1)$$

with transition temperatures slightly depending on cell gap. This is not of relevance to the present studies, as these were carried out as function of quench depth—i.e., temperatures reduced to the respective clearing point.

The phase ordering process at the iso–Sm-*C* transition was investigated by quenching the sample below the transition temperature to a quench depth ΔT and recording polarizing microscopic images as a function of time (Nikon Optiphot-Pol, equipped with digital image acquisition, JVC model KY-F1030U). The temperature of the sample was controlled to an accuracy of 0.1 K by a Linkham THMS600 hot stage and a TP92 controller. Investigations were carried out in commercially available liquid crystal sandwich cells (E.H.C., Japan) with planar polyimide alignment layers, varying the cell gap d between 2 and 15 μm. Lateral cell dimensions were 15 mm $\times$ 10 mm. We were thus effectively investigating two-dimensional growth behavior, which justifies the two-dimensional fractal analysis presented below. In all cases the fractal aggregates were clearly larger than the cell gap. The quench depth ΔT was varied between 0.1 and 0.8 K; for larger quench depths, growth could not be achieved at isothermal conditions. The quench rate R was varied between 1 and 3 K min^{-1} and was adopted to 3 K min^{-1} for most results shown below. This quench rate gave the best compromise between temperature control and achievable quench depth for isothermal growth, although it should be mentioned that the same results were also obtained for smaller quench rates.

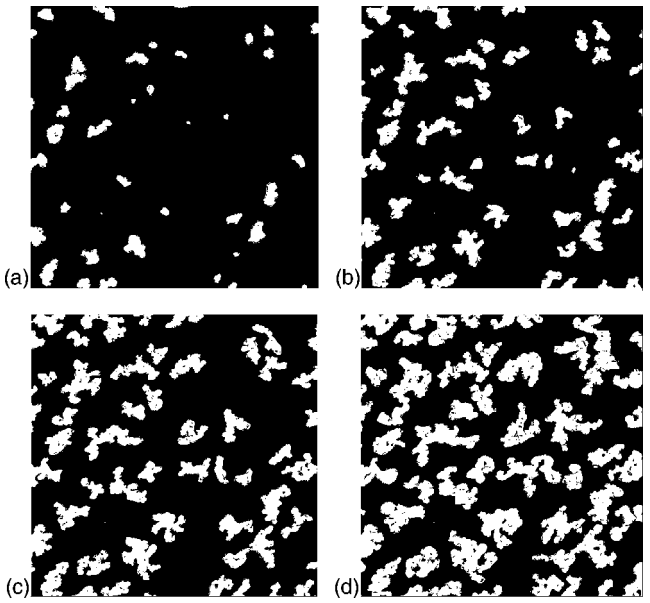

FIG. 1. Illustration of a typical time series of 8DBH growth aggregates obtained at isothermal conditions after a temperature quench below the isotropic to Sm-*C* transition ($R=3$ K min^{-1}, $\Delta T=0.8$ K, $d=2$ μm). White areas represent the liquid crystal Sm-*C* phase, growing from the black isotropic background. The image size is 390 μm $\times$ 390 μm; (a) $t=15$ s, (b) $t=20$ s, (c) $t=25$ s, and (d)$t=50$ s.

B. Fractal analysis

Digital images were recorded at a relatively high resolution of 1280 $\times$ 960 pixels, corresponding to an image size of 520 μm $\times$ 390 μm. This ensured that the digital resolution of the camera did not represent the limiting factor in the fractal analysis, but that resolution was indeed only limited by the optical microscopic method employed, which is on the order of 1 μm. Figure 1 shows a typical texture time series of the isothermal growth structures observed, scaled to 390 μm $\times$ 390 μm for later comparison to textures simulated on a square grid. For the fractal analysis the recorded textures were converted from color to gray scale images and further to binary images by manual thresholding with software IMAGETOOL 3.0, developed at the University of Texas Health Science Center, San Antonio. During image acquisition the camera was driven in slight overload to assure good contrast between the liquid crystal aggregates and the isotropic phase. Care was taken that all images were clearly in focus during texture recording. The image conversion process was carried out manually for each individual image,

assuring that all structural features of the aggregates were maintained. Fractal analysis [17–20] was carried out with software BENOIT1.3 (TruSoft International) on single aggregates as well as whole textures, both leading to the same fractal dimension and thus indicating dilatation invariance. Two analysis methods were employed, the *information dimension method* and the *ruler dimension method*. The information dimension D_i is related to the mass of an object—i.e., the capability of filling two-dimensional space—and is defined from the proportionality

$$I(d) \sim -D_i \ln(d), \tag{1}$$

with

$$I(d) = -\sum_{i=1}^{N(d)} m_i \ln(m_i), \tag{2}$$

where $m_i = M_i/M$, with M_i the number of points in the ith box and M the number of total points in the data set. The information dimension method is essentially equivalent to the commonly employed box dimension (D_b) method, described by

$$N(d) \sim \frac{1}{d^{D_b}}, \tag{3}$$

with $N(d)$ being the number of occupied boxes of side length d. In contrast to the box dimension method, the information dimension method weights the object pixel content of a box. Whereas for the box dimension an individual box counts towards $N(d)$ even if just a single object pixel is contained within this box, the information dimension method weights the object pixel content within each box. It thus minimizes errors through "stray" pixels, which are present in every image of a natural, nonmathematical structure. It is $D_i \geqslant D_b$ and $1 < D_i < 2$ characterizes a fractal image in two-dimensional space. If $D_i = 2$, the aggregate is space filling and Euclidian. The information dimension method can be used for the analysis of single aggregates as well as for whole textures.

The ruler dimension D_r is related solely to the perimeter of an object. It is defined from the proportionality

$$M(l) \sim l^{-D_r}, \tag{4}$$

with $M(l)$ being the number of steps a ruler of length l has to be taken around the perimeter of an object, which has to be a closed loop. The ruler dimension method can thus only be used for the analysis of single aggregates and gives $1 < D_r < 2$ for a fractal object. $D_r = 1$ characterizes a Euclidean line.

Both methods are demonstrated for a typical single 8DBH cluster shown in Fig. 2. Figure 3(a) illustrates the employment of the information dimension method, exhibiting scaling according to Eqs. (1) and (2) over more than two decades of box side length and four decades of the dependent variable. It is commonly accepted practice in the fractal analysis of natural patterns to disregard very large as well as very small box sizes. Experience has shown that the most reliable fractal dimensions are extracted from box sizes d between approximately 1/10 of the maximum size of the image as the large box size limit and 10 times the image pixel size as the low-box-size limit. This rule of thumb was also applied in the present investigations, making further discussions with respect to optical resolution unnecessary. The experimentally determined information dimension is $D_i = 1.89$, obtained from a linear fit to the data with a minimized standard deviation SD < 0.001. D_i is precisely equal to the theoretical value ($D_i = 91/48$) expected for two-dimensional percolation growth at the percolation threshold. Figure 3(b) illustrates the ruler dimension method for the same cluster (Fig. 2),

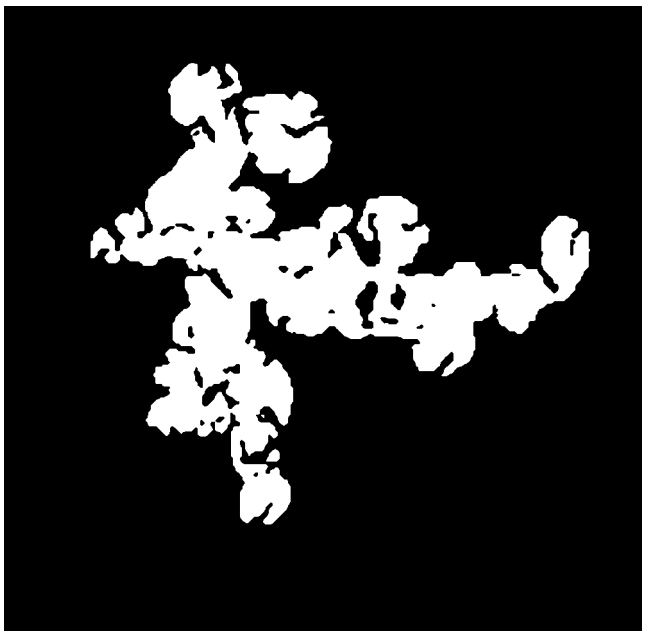

FIG. 2. A typical single-liquid-crystal Sm-C growth aggregate of 8DBH, used for the illustration of the different fractal dimension methods employed in this study (see Fig. 3).

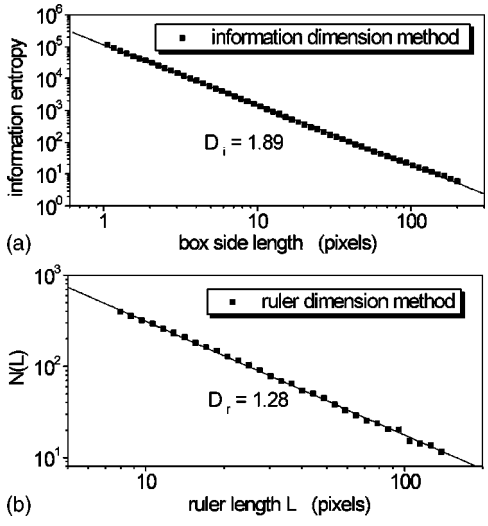

FIG. 3. Demonstration of the different methods employed in the fractal dimensional analysis, applied to the aggregate depicted in Fig. 2. (a) The information dimension method [Eqs. (1) and (2)], relating to the mass of the aggregate, and (b) the ruler dimension method [Eq. (3)], relating to the perimeter of the aggregate. Fractal scaling is observed over at least two orders of magnitude.

with $D_r = 1.28$ clearly evidencing that also the perimeter of the observed clusters is fractal.

C. Computer simulations

Computer simulations of the observed growth were carried out for single clusters as well as multicluster textures. In the former case a 600×600 pixel square grid was used with a single-site nucleation center, while in the latter case a 1200×1200 pixel square grid was used with nucleation sites occurring at random. For all simulations a standard percolation algorithm was employed, which can be outlined as follows: (i) In a first step the seed particle is set (this occurs at random positions for multisite percolation). (ii) All nearest neighbors (square grid sites sharing a common side with the seed particle) are identified and set "alive"—i.e., can potentionally be occupied. (iii) Alive sites are occupied at random with an occupation probability p and "killed" with a probability $1-p$. Occupied sites are part of the growing cluster, while killed sites cannot be occupied in any of the further iteration steps; i.e., they are "dead." (iv) The new nearest neighbors are identified (while ignoring dead sites), set alive, and steps (iii) and (iv) of the algorithm are carried out for many iterations until the growing cluster reaches one of the edges of the grid. For the multisite percolation simulations to generate the actually observed textures (not only the single aggregates) the latter stop condition was abandoned, being equivalent to an infinite two-dimensional sample. This situation is reasonably well achieved experimentally, as the investigated cell gaps are by several orders of magnitude smaller than the lateral dimensions of the sample sandwich cell.

Initial computer simulations were carried out at variable occupation probabilities p to confirm that the percolation threshold p_c of the simulations corresponds to the theoretically predicted value of $p_c = 0.593$. This was indeed the case, as clusters with a lower occupation probability $p < p_c$ did not grow indefinitely. In accordance with the experiments, the time development of either a single cluster or multiple clusters was investigated by terminating the simulation algorithm after a varying number of iteration steps. Computer-generated growth structures were analyzed with respect to their fractal dimension according to the methods outlined above.

III. RESULTS AND DISCUSSION

A. Experimental results

A first step in the analysis of experimentally obtained fractal growth structures has to be the confirmation of dilatation invariance. For this reason Fig. 4(a) depicts an example of the time evolvement of the fractal dimensions D_i and D_r of a single 8DBH cluster at a quench depth of $\Delta T = 0.6$ K and cell gap $d = 15$ μm. Parameters were chosen to demonstrate that fractal growth is not induced by the boundary conditions of the substrates, as liquid crystals behave bulk like for cell gaps larger than approximately 8 μm. The information dimension D_i quickly saturates at a value of $D_i = 1.9$, a behavior which is observed for all of the time series

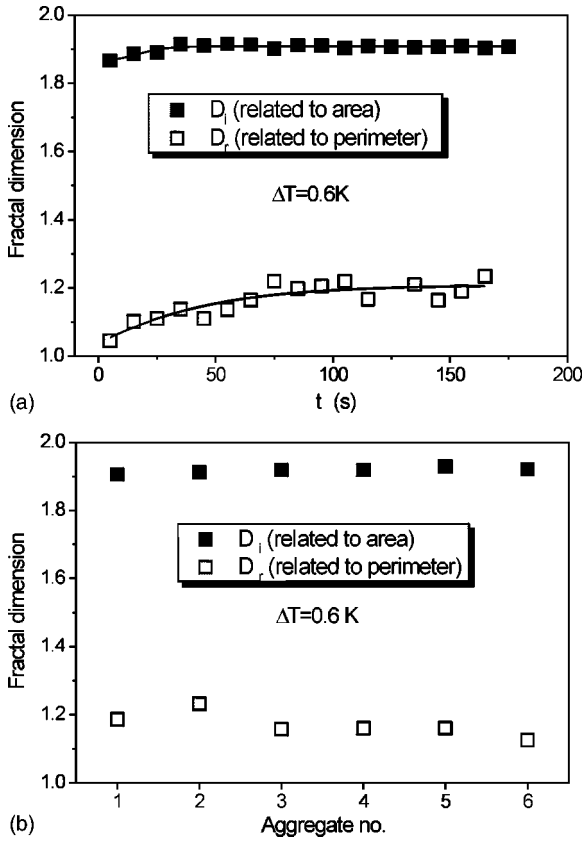

FIG. 4. (a) Time evolution of the fractal dimensions D_i and D_r determined from the growth of a single aggregate. Values of the fractal dimensions reach saturation after approximately 60 s. (b) Information dimension D_i and ruler dimension D_r for several different aggregates of varying size between 15 μm and 500 μm. The fact that within the limits of error all aggregates exhibit equal fractal dimensions illustrates dilatation invariance.

investigated at various applied growth conditions. Also the ruler dimension D_r is found to exhibit saturation behavior. Figure 4(b) shows the values of D_i, related to the mass of the fractal, and D_r, related to its perimeter, for six different aggregates of 8DBH at varying size between 15 μm and 500 μm, growing under identical experimental conditions. It is worth noting that the fractal dimension determined for individual aggregates is equal to that of the whole texture, so coalescence of aggregates is not a critical issue. Within the limits of error, which are estimated to ± 0.01 for D_i and ± 0.03 for D_r, the saturation fractal dimensions are found to be equal for all different aggregates, illustrating dilatation invariance.

In the following we concentrate our discussion on the analysis of whole texture images, varying the quench rate R, the quench depth ΔT, and the sample cell gap d. Figure 5 summarizes the time development of the fractal dimension D_i for various quench conditions. Figure 5(a) shows the evolution of $D_i(t)$ as a function of quench rate R for the two extreme cell gaps of $d = 2$ μm and $d = 15$ μm at a quench depth of $\Delta T = 0.5$ K. In all cases the fractal dimension reaches saturation, a process which seems to be faster for large cell gaps than for small ones. The quench rate R does not have any influence on the saturation fractal dimension,

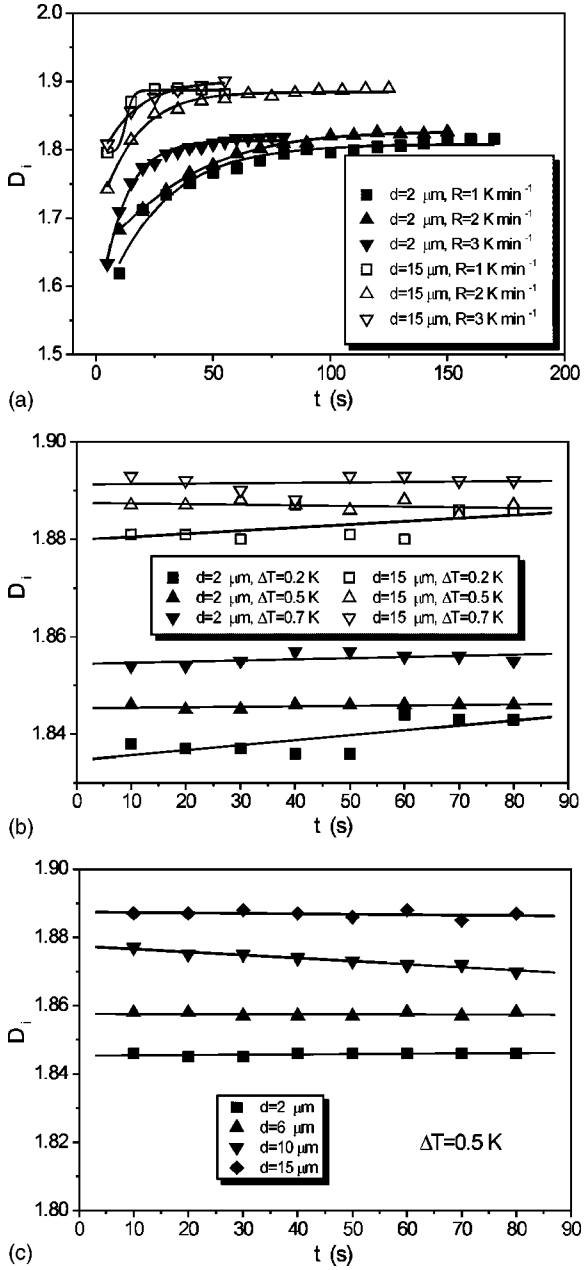

FIG. 5. Fractal information dimension D_i as a function of time for (a) varying quench rate R at $\Delta T=0.5$ K for a thin cell (solid symbols, $d=2$ μm) and a thick cell (open symbols, $d=15$ μm), (b) varying quench depth ΔT at $R=3$ K min^{-1} for a thin cell (solid symbols, $d=2$ μm) and a thick cell (open symbols, $d=15$ μm), and (c) varying cell gap d at quench depth $\Delta T=0.5$ K and $R=3$ K min^{-1}.

which is $D_i=1.8$ for the thin cell and $D_i=1.9$ for the thick cell, the latter value being the one expected for percolation growth at the percolation threshold. This gives a first indication that the growth process may be slightly influenced by the boundary layers in the case of the 2-μm cell, while the 15-μm cell exhibits bulklike behavior.

Figure 5(b) depicts the time dependence of the fractal dimension D_i as a function of quench depth ΔT, again for the two extreme cell gaps of $d=2$ μm and $d=15$ μm at a quench rate of $R=3$ K min^{-1}. A slight increase of the fractal dimension with increasing quench depth ΔT is observed, but it should be noted that this is indeed close to the limits of error, although the same trend is shown in both cell gap series. Again, values for the thin cell are smaller than those of the thick cell, which suggests that the fractal dimension D_i does in fact exhibit a dependence on cell gap d, which will be discussed below. We note that the fractal dimension determined for relatively large quench depth and cell gap again precisely exhibits the value expected for percolation growth at the percolation threshold ($D_i=1.89$).

Figure 5(c) finally shows $D_i(t)$ as a function of cell gap d at a quench depth $\Delta T=0.5$ K and a quench rate $R=3$ K min^{-1}. Saturation is quickly achieved and the fractal dimension of the studied textures clearly increases with increasing cell gap. Again, $D_i=1.89$ is observed for the thick cell.

The results indicate that the textures observed for increasing quench depth and cell gap approach the theoretically expected value of $D_i=91/48=1.896$ for percolation growth at the percolation threshold p_c. We have thus carried out more detailed investigations of the quench depth and cell gap dependence of the saturation fractal dimension of D_i. Figure 6(a) shows D_i as a function of quench depth ΔT for the two extreme cell gaps of $d=2$ μm (circles) and $d=15$ μm (diamonds), over the whole range of quench depths that assured isothermal phase ordering. For the thin cell the fractal dimension slowly increases, while the thick cell exhibits a quick increase of the fractal dimension with quench depth, reaching saturation of $D_i=1.89$ at approximately $\Delta T=0.4$. The error bars represent a rather conservative estimation of D_i to ± 0.01, which is the range of data reproducibility. This is much larger than the standard deviation, which was minimized to SD$\leqslant 0.001$ in the determination of the fractal dimension from linear fits to the relations of Eqs. (1) and (2).

Figure 6(b) depicts the respective cell gap dependence of D_i at a quench depth of $\Delta T=0.5$ K. The fractal dimension increases with increasing cell gap, as was also observed in previous phase ordering studies of bent-core molecules [12], although we here do not as quite observe the saturation behavior above approximately $d=8$ μm. The overall obtained experimental results from a variety of different investigation series on 8DBH show that the fractal dimensions of growth aggregates and textures all converge towards a value of $D_i=1.89\pm 0.01$ at large cell gaps d, quench depths ΔT, and quench rates R. This is precisely the theoretically predicted value of two-dimensional percolation growth at the percolation threshold. In the following section we report computer simulations to further verify this conclusion.

B. Comparison to computer simulations

The algorithm employed is a site percolation model as outlined above. Single clusters were simulated at varying site occupation probability p and it was confirmed that growth stopped at very small clusters sizes if $p<0.58$. Only for occupation probabilities above the theoretically predicted percolation threshold of $p>p_c=0.59$ were large growing clusters obtained. Figure 7(a) shows one of the simulated clusters for an occupation probability just above the percola-

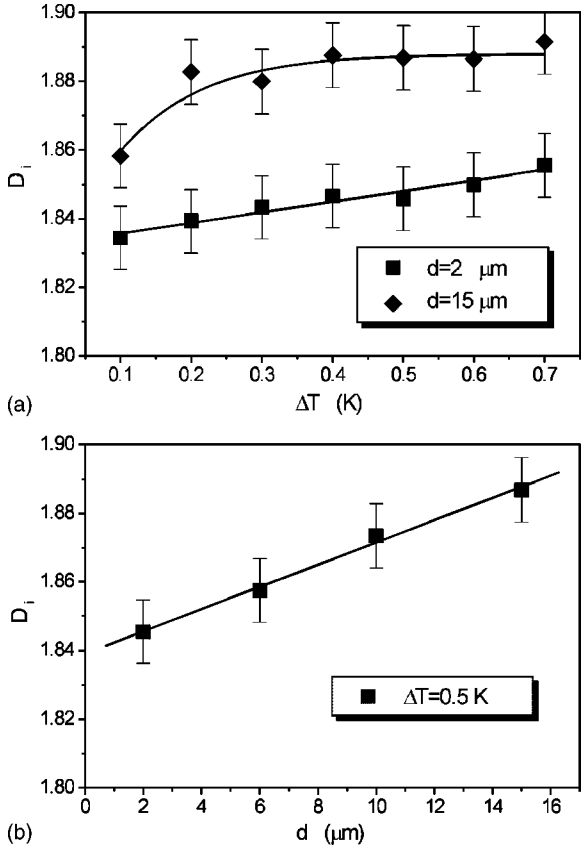

FIG. 6. (a) Saturation fractal information dimension D_i as a function of quench depth ΔT for a thin cell ($d=2$ μm, squares) and a thick cell ($d=15$ μm, diamonds). In the case of the thick cell the fractal dimension approaches $D_i=1.89$, the theoretically predicted value for two-dimensional percolation growth at the percolation threshold. (b) Saturation fractal information dimension D_i as a function of cell gap d.

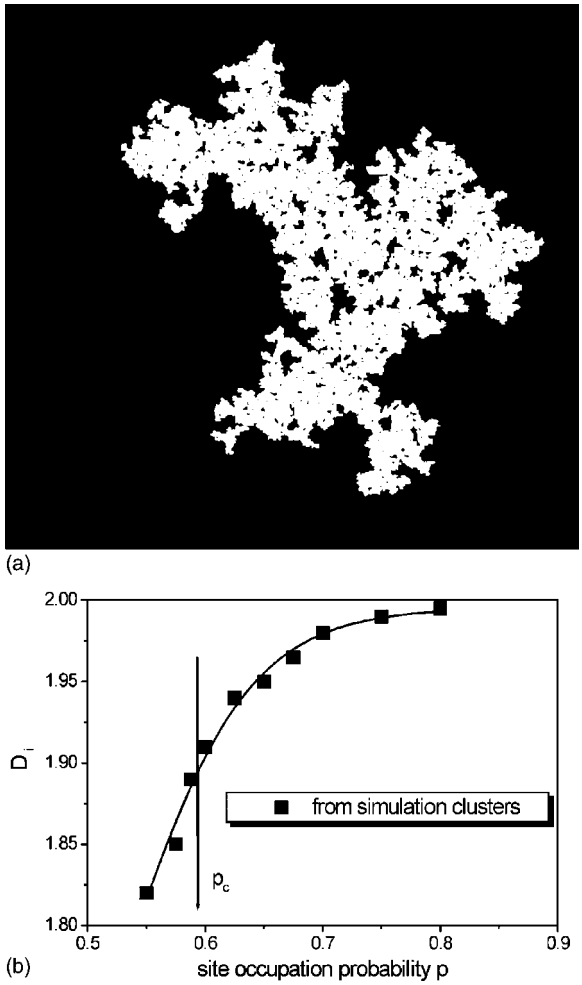

FIG. 7. (a) Simulated growth aggregate for a site occupation probability of $p=0.625$, just above the percolation threshold. The generated cluster is very similar to the experimentally obtained aggregates (compare to Fig. 2). (b) Fractal information dimension D_i as a function of site occupation probability p. Below the percolation threshold at $p_c=0.59$ clusters are not growing indefinitely. The saturation fractal dimensions obtained from the experimental clusters and textures (Figs. 4 and 5, $D_i \approx 1.9$) suggest percolation growth in the vicinity of the percolation threshold.

tion threshold with $p=0.625$. The generated cluster is very similar in appearance to those observed experimentally (see Fig. 2) and indeed within the limits of error exhibits the same fractal dimensions $D_i=1.89$ and $D_r=1.3$ (see Fig. 3). Comparing the experimentally determined fractal dimensions of the previous section to those of Fig. 7(b), which shows the information dimension D_i obtained from cluster images simulated at varying site occupation probability p, it can clearly be deduced that 8DBH growth is accomplished via percolation in the close vicinity of the percolation threshold.

The time evolution of a growing texture can be simulated by halting the generic computer algorithm of multisite percolation after a varying number of iteration steps. Illustrative images of such a time series simulation are depicted in Fig. 8(A) for a site occupation probability of $p=0.625$. The computer-generated texture images of Fig. 8(A) clearly mimic the experimentally obtained textures of Fig. 1. As a quantitative measure, the respective time evolvement of the fractal dimension D_i is shown in Fig. 8(B). This mirrors that of the experimentally observed behavior (Figs. 4 and 5) giving clear evidence for percolation growth close to the percolation threshold of the conventional calamitic 8DBH mesogen.

We can thus confidently conclude that fractal growth of a conventional calamitic smectic mesophase has been demonstrated and that its growth mechanism is related to percolation at the percolation threshold. The phase formation behavior of calamitic 8DBH is qualitatively and quantitatively very similar to that observed for "banana" or bent-core liquid crystals [28]. In the following section we will discuss the possible molecular reasons for this similarity as contrasted by all other calamitic smectic growth structures, especially smectic bâtonnet growth.

C. Discussion

For calamitic (rodlike) molecules, the general growth behavior of smectic phases from the isotropic melt is observed

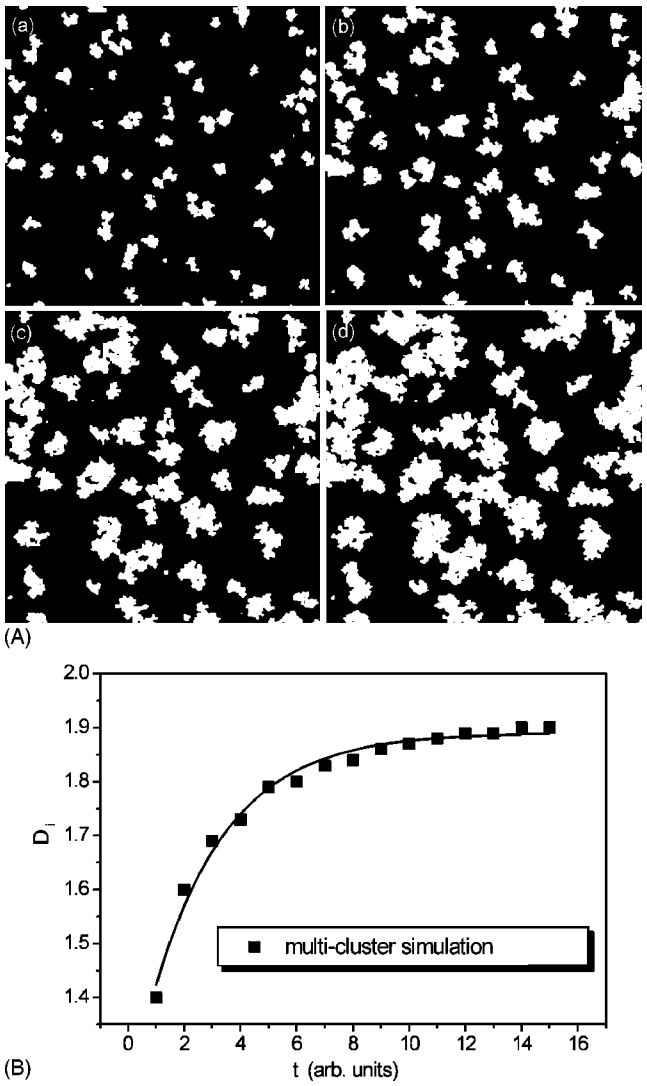

FIG. 8. (A) Computer-generated time series of the texture evolvement at isothermal growth conditions according to a multisite percolation model with $p=0.625$. The images mimic those of the experimentally obtained time series of Fig. 1. (B) Time dependence of the fractal information dimension D_i, obtained from multisite percolation texture generation. The behavior is equivalent to that observed in the experiments [see Fig. 5(a)]. The accordance of results from the computer simulations with the experimental data provides strong evidence for percolation growth at the percolation threshold being the responsible mechanism in the phase ordering process of the 8DBH aggregates.

via the nucleation and anisotropic growth of so-called bâtonnets [14]. Growth perpendicular to the smectic layer plane—i.e., along the smectic normal—is much more pronounced than growth in direction of the layer plane, resulting in shape anisotropic aggregates [29,30] with an aspect ratio in the order of 5:1. This means that the process of smectic layer formation is favored over the growth within individual layers.

The here investigated calamitic mesogen 8DBH is in some respects different from the majority of other calamitic mesogens, as it promotes the formation of hydrogen bonds perpendicular to its long molecular axis—i.e., in the plane of the smectic layers. This is also exemplified by the formation of the cubic phase of 8DBH at somewhat lower temperatures. This hydrogen bonding within the layer plane is relatively strong in comparison to the general van der Waals interactions between anisotropic molecules in a direction perpendicular to their long axis. We suggest that this is the reason for the breaking of the anisotropy in interactions being responsible for smectic layer formation and growth within a smectic layer, as is observed for the majority of conventional calamitic mesogens. In the context of a generic growth model, this implies that the site occupation probabilities are independent of direction—i.e., are isotropic—a condition as was employed in the computer simulations presented above. The fact that quench experiments were carried out into the two-phase region accounts for the site occupation probability being smaller than 1 (isotropic regions representing the "dead" sites). It is important to note that the same qualitative arguments also hold for the fractal growth of the smecticlike phases of bent-core molecules, especially the $B2$ phase [12,28]. In the latter case the strong intermolecular interactions within the smectic layer plane, as provided by hydrogen bonding for 8DBH, are instead caused by steric interactions due to the bent-core molecular shape. As in the case for 8DBH, this leads to a percolation growth mechanism, which results in growth and texture formation via fractal aggregates of a dimension $D \approx 1.9$, as is observed in experiments.

IV. CONCLUSIONS

The isothermal growth process of the smectic-C phase of 8DBH from the isotropic melt was experimentally investigated for a conventional calamitic mesogen with respect to quench depth, quench rate, and cell gap. The observed growth structures exhibit a saturation fractal dimension of $D=1.9$, showing fractal growth in a conventional calamitic mesophase. Site percolation at the percolation threshold is suggested as the generic formation mechanism of the experimentally observed liquid crystalline textures. This is supported by computer simulations carried out according to a multisite percolation algorithm, which qualitatively and quantitatively generates equivalent growth aggregates and textures. It is proposed that in the case of 8DBH hydrogen bonding is the responsible mechanism for the formation of fractal aggregates, while the model can easily be extended to also explain the fractal growth of the $B2$ phase of bent-core mesogens through steric interactions.

ACKNOWLEDGMENTS

We would like to express our sincere thanks to W. Weissflog, who generously provided the liquid crystal investigated in this study. Financial support from The Nuffield Foundation under Grant No NAL/00680/G is also gratefully acknowledged.

[1] L. Ratke and P. W. Voorhees, *Growth and Coarsening* (Springer, Berlin, 2002).
[2] P. C. Hohenberg and B. I. Halperin, Rev. Mod. Phys. **49**, 435 (1977).
[3] A. J. Bray, Adv. Phys. **43**, 357 (1994).
[4] P. Meakin, *Fractals, Scaling and Growth Far From Equilibrium* (Cambridge University Press, Cambridge, England, 1998).
[5] T. Vicsek, *Fractal Growth Phenomena* (World Scientific, Singapore, 1989).
[6] *Soft Matter Physics*, edited by M. Daoud and C. E. Williams (Springer, Berlin, 1999).
[7] M. Kleman and O. D. Lavrentovich, *Soft Matter Physics* (Springer, New York, 2003).
[8] I. Dierking, ChemPhysChem **2**, 59 (2001).
[9] T. Sekine, T. Niori, M. Sone, J. Watanabe, S. W. Choi, Y. Takanishi, and H. Takezoe, Jpn. J. Appl. Phys., Part 1 **36**, 6455 (1997).
[10] D. R. Link, G. Natale, R. Shao, J. E. Maclennan, N. A. Clark, E. Körblova, and D. M. Walba, Science **278**, 1924 (1997).
[11] G. Pelzl, S. Diele, and W. Weissflog, Adv. Mater. (Weinheim, Ger.) **11**, 707 (1999).
[12] I. Dierking, J. Phys.: Condens. Matter **13**, 1353 (2001).
[13] I. Dierking, H. Savade, and G. Heppke, Liq. Cryst. **28**, 1767 (2001).
[14] I. Dierking, *Textures of Liquid Crystals* (Wiley-VCH, Weinheim, 2003).
[15] J. Thisayukta, Y. Nakayama, S. Kawauchi, H. Takezoe, and J. Watanabe, J. Am. Chem. Soc. **122**, 7441 (2000).
[16] I. Dierking, Physica B **304**, 51 (2001).
[17] B. Mandelbrot, *The Fractal Geometry of Nature* (Freeman, San Francisco, 1982).
[18] *Fractals in Science*, edited by A. Bunde and S. Havlin (Springer, Berlin, 1994).
[19] *Fractals and Disordered Systems*, edited by A. Bunde and S. Havlin (Springer, Berlin, 1996).
[20] B. H. Kaye, *A Random Walk Through Fractal Dimensions*, 2nd ed. (VCH, Weinheim, 1994).
[21] T. A. Witten and L. M. Sander, Phys. Rev. Lett. **47**, 1400 (1981).
[22] P. Meakin, Phys. Rev. Lett. **51**, 1119 (1983).
[23] D. Stauffer and A. Aharony, *Introduction to Percolation Theory* (Taylor & Francis, London, 1992).
[24] M. Sahimi, *Applications of Percolation Theory* (Taylor&Francis, London, 1994).
[25] H. Schubert, J. Hauschild, D. Demus, and S. Hoffmann, Z. Chem. **18**, 256 (1978).
[26] D. Demus, A. Gloza, H. Hartung, A. Hauser, I. Rapthel, and A. Wiegeleben, Cryst. Res. Technol. **16**, 1445 (1981).
[27] P. Göring, S. Diele, S. Fischer, A. Wiegeleben, G. Pelzl, H. Stegemeyer, and W. Thyen, Liq. Cryst. **25**, 467 (1998).
[28] I. Dierking, Liq. Cryst. Today **12**, 1 (2003).
[29] I. G. Chistyakov, Kristallografiya **8**, 123 (1963).
[30] I. Dierking and C. Russell, Physica B **325**, 281 (2003).